ADVANCED HEALTHCARE MATERIALS
www.advhealthmat.de

Growth Hormone-Loaded 3D Printed Silk Fibroin-Cellulose Dressings for Ischemic Wounds

Maria Pita-Vilar, Diego Caicedo-Valdés, Susana B. Bravo, Isabel Rodriguez-Moldes, Salvador D. Aznar-Cervantes, Angel Concheiro, Carmen Alvarez-Lorenzo, and Luis Diaz-Gomez**

In this study, carboxymethyl cellulose-silk fibroin (CMC-SF) wound dressings loaded with growth hormone (GH) are developed for chronic wound care, particularly in diabetic ulcer regeneration. Designed with a porous and reproducible structure, the dressings enable rapid, localized GH release within 24 h and maintain high fluid absorption with minimal swelling, ensuring optimal conformity to the wound site. The inclusion of SF and GH significantly enhances cell proliferation, migration, and angiogenesis in vitro. The dressings also enable nontraumatic removal, as demonstrated in an in ovo model, supporting their suitability for clinical applications. In vivo testing in ischemic diabetic wounds shows accelerated tissue regeneration, reduced scarring, and improved healing quality. Proteomics and immunohistochemical analyses indicate that GH contributes to a more balanced inflammatory response, enhanced antioxidant activity and vascularization, and better regulation of tissue remodeling processes. Overall, the incorporation of GH within the CMC-SF dressings represents a promising and effective approach to support diabetic ulcer regeneration.

1. Introduction

Personalization, sustainability, and bioactivity are key demands in modern wound dressings.[1] In addition to other manufacturing techniques, 3D printing has gained attention in skin tissue regeneration, enabling on-demand production of dressings with porosities and shapes tailored to specific structural and functional needs.[2–4] The ideal pore size varies with wound characteristics: smaller pores suit high exudate wounds, while larger pores work better for drier wounds. Optimizing pore size at the wound-contact interface is key to regulating exudate flow and preventing fibroblast and keratinocyte infiltration, reducing tissue damage during dressing changes.[5,6]

Growing concerns over healthcare waste and microplastic pollution highlight the need for natural, sustainably sourced materials. Hydrogels made from natural proteins and polysaccharides, like cellulose derivatives, can mimic the fibrillar architecture of the extracellular matrix, making them especially appealing for bioprinting applications.[7,8] Their hydrophilicity, suitable mechanical strength, and good permeability to oxygen and nutrients make them strong candidates for next-generation dressings.[9]

M. Pita-Vilar, A. Concheiro, C. Alvarez-Lorenzo, L. Diaz-Gomez
Departamento de Farmacología
Farmacia y Tecnología Farmacéutica
I+D Farma Group (GI-1645)
Facultad de Farmacia
Instituto de Materiales (iMATUS) and Health Research Institute of Santiago de Compostela (IDIS)
Universidade de Santiago de Compostela
Santiago de Compostela 15782, Spain
E-mail: carmen.alvarez.lorenzo@usc.es; luis.diaz.gomez@usc.es

The ORCID identification number(s) for the author(s) of this article can be found under https://doi.org/10.1002/adhm.202502969

DOI: 10.1002/adhm.202502969

D. Caicedo-Valdés
Department of Vascular Surgery
Health Research Institute of Santiago de Compostela (IDIS)
School of Medicine
Universidade de Santiago de Compostela
Santiago de Compostela, A Coruña 15782, Spain

S. B. Bravo
Proteomic Unit
Health Research Institute of Santiago de Compostela (IDIS)
Santiago de Compostela, A Coruña 15706, Spain

I. Rodriguez-Moldes
Grupo NEURODEVO
Departamento de Bioloxía Funcional
Universidade de Santiago de Compostela
Santiago de Compostela 15782, Spain

S. D. Aznar-Cervantes
Biotechnology Team
Murcian Institute of Agricultural and Environmental Research and Development (IMIDA)
La Alberca, Murcia 30150, Spain

Silk fibroin (SF) has been widely evaluated for its ability to support cell adhesion, wound contraction, re-epithelialization, angiogenesis, and collagen formation, without triggering an immune response. FDA-approved SF-based products, including cosmetics and dressings like D-FIBROHEAL Ag, have already been introduced to the market.[10] SF can be functionalized or combined with therapeutic agents, including drugs, peptides, and non-protein growth factors, to enhance its angiogenic potential.[11,12] However, processing SF into complex structures is difficult due to its low viscosity in solution and the poor mechanical strength of the resulting dressings.[13] These limitations can be addressed by blending SF with polysaccharides.[14] The incorporation of SF into hydrogels has emerged as a promising strategy, enhancing their malleability, imparting antibacterial properties, facilitating underwater adhesion, and improving both real-time self-healing and water-sealing capabilities.[15] SF combined with chitosan or cellulose derivatives such as carboxymethyl cellulose (CMC) and nanocellulose has been used to fabricate 3D-printed constructs for wound healing applications.[16]

CMC-based inks offer tunable viscosity, improving printability and enabling defined porous scaffolds for personalized treatment.[17,18] Additionally, the incorporation of growth factors and hormones can enhance wound healing;[19] notably, growth hormone (GH or somatropin) has been shown to directly promote wound repair by many mechanisms, such as the activation of vasodilation and angiogenesis through the nitric oxide pathway.[20] Furthermore, its direct and indirect actions (influencing other key pathways, such as IGF-1),[21] are also particularly important for modulating cell proliferation and migration, especially in fibroblasts, keratinocytes, and endothelial cells, all of which play crucial roles in wound contraction and healing.[22,23] This makes diabetic ulcers strong candidates for GH-loaded wound dressings, as their poor healing is due to two main mechanisms: neuropathy and vascular ischemia, and GH has been demonstrated to improve nerve function at the wound, which is essential for healing.[24–26]

This study aimed to develop personalized GH-loaded dressings by optimizing the printability and stability of CMC-SF ink. It is hypothesized that the local release of GH within the wound bed by this method can enhance skin regeneration in chronic wounds, particularly in diabetic ulcers, accelerating and improving tissue regeneration. By combining the structural function of the dressing as a physical support with GH and SF as bioactive agents, this work proposes an innovative therapeutic strategy: an advanced local delivery platform capable of modulating the wound microenvironment.

Printable CMC-SF blends were selected based on their rheological properties and fabricated into porous wound dressings for further characterization. Cytocompatibility and wound closure were assessed in vitro, while angiogenic potential was preliminarily evaluated using an in ovo model. In vivo efficacy was tested in an ischemic wound model in diabetic rats. Histological and proteomic analyses were performed to investigate the mechanisms underlying tissue regeneration. Proteomics has become a powerful tool in wound healing research, providing direct insights into the functional proteins and post-translational modifications that regulate key processes such as cell behavior, inflammation, angiogenesis, and extracellular matrix remodeling, beyond what transcriptomics can reveal.[27,28] This level of molecular detail is particularly valuable in chronic wounds, such as diabetic ulcers, where dysregulation of specific proteins can impair healing and lead to prolonged inflammation or fibrosis.[29,30]

2. Results and Discussion

2.1. Ink Characterization

In this work, 3D-printed wound dressings based on CMC-SF composite inks were developed and functionalized with growth hormone to promote diabetic ulcer regeneration through enhanced bioactivity and structural performance. SF was incorporated for its well-documented regenerative properties, including the promotion of neovascularization, attenuation of inflammatory responses, and enhancement of local microcirculation at the wound site.[31] Despite these advantages, the direct 3D printing of SF remains technically challenging due to its inherently low viscosity and slow gelation kinetics, which hinder the structural fidelity of printed constructs. To overcome these limitations, CMC was employed as the primary matrix material, offering improved printability alongside favorable wound dressing properties such as high exudate absorption capacity, biocompatibility, and minimal immunogenicity.[17] A high molecular weight CMC (395 kDa, degree of substitution 0.9) was specifically selected to provide mechanical support and structural integrity. Additionally, citric acid (CA) was introduced as a cross-linking agent to enhance the mechanical robustness and long-term stability of the printed constructs through esterification of CMC at 120 °C.[32]

Cyclic strain sweeps were performed to evaluate ink behavior at rest, under extrusion-like shear, and post-extrusion.[19] All inks showed significant drops in both storage (G') and loss (G'') moduli under high strain (100%), with G' decreasing more markedly (**Figure 1**). Upon returning to rest conditions (0.5% strain), G' rapidly recovered, demonstrating self-healing behavior with > 85% recovery after three cycles, confirming good printability. Increasing CMC concentration enhanced G', indicating a stronger hydrogel structure.[19,33] The optimal CMC concentration in water was determined to be 15 w/v%, ensuring adequate printing properties. 10 w/v% CMC inks showed poor printability, while 20 w/v% CMC ink was too viscous and trapped air bubbles. To incorporate SF while maintaining suitable rheology, CMC concentration was adjusted. A 6 w/v% CMC combined with 5 w/v% SF (CMC6-SF5) yielded stable, continuous fibers, avoiding clogging or collapse observed with higher or lower CMC concentrations. Therefore, CMC6-SF5 was chosen for the preparation of the wound dressings, showing comparable G' and printability to the CMC15 ink in both self-healing and filament extrusion tests (Figure S1, Supporting Information).

2.2. Structural Characterization

The microstructure of the 3D-printed CMC and CMC-SF dressings was observed using scanning electron microscopy (SEM) and micro-CT (**Figure 2A–F**). Both compositions showed excellent print fidelity with well-defined macropores in the 530–550 µm range and homogeneous microporosity throughout the

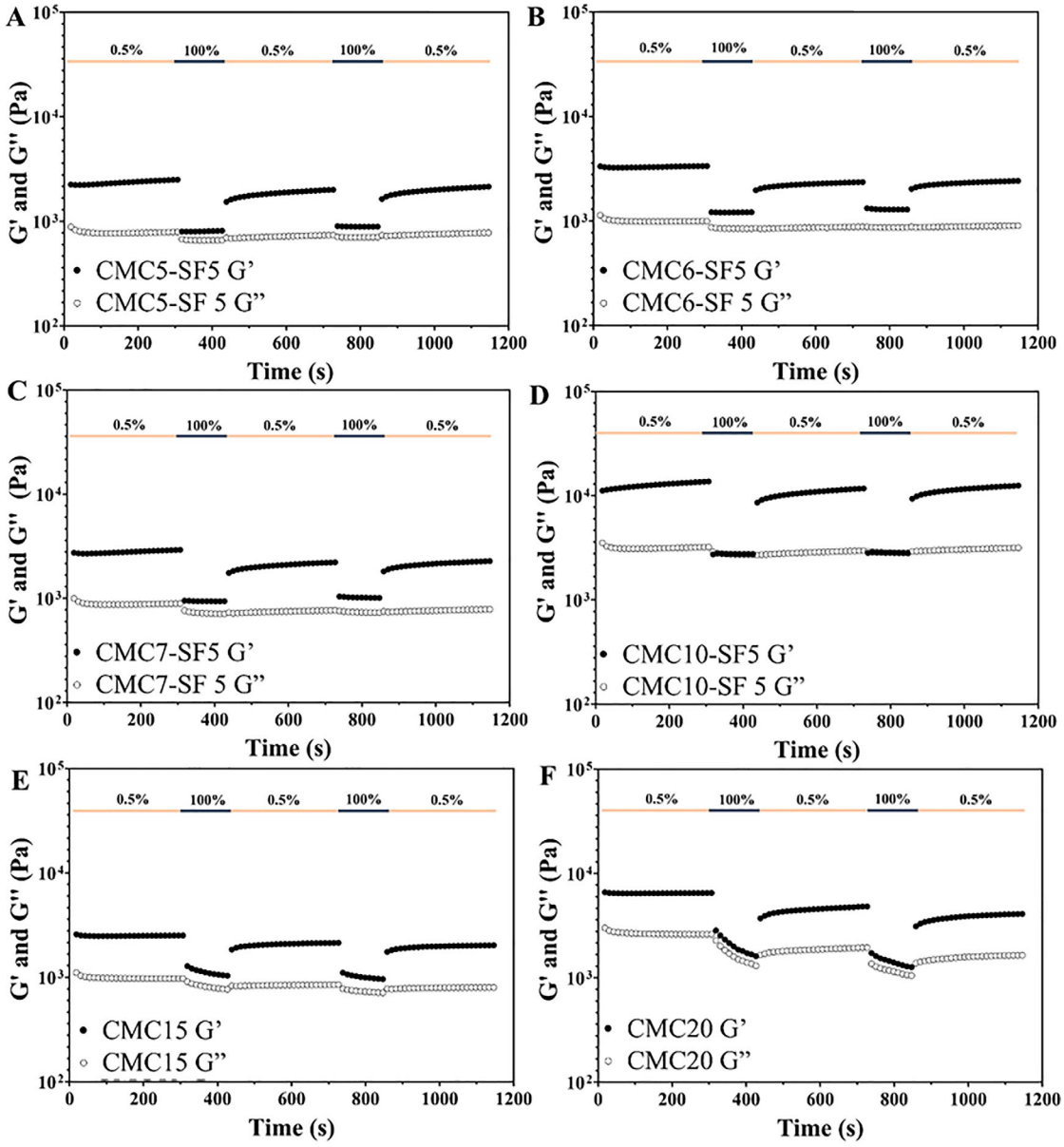

Figure 1. Rheological behavior of CMC and CMC-SF inks (A: CMC5-SF5; B: CMC6-SF5; C: CMC7-SF5; D: CMC10-SF5; E: CMC15, F: CMC20) under cyclic changes in shear strain, namely 0.5% (simulating resting position) and 100% (mimicking the shear stress at the nozzle tip during ink extrusion) at 20 °C.

printed fibers. Quantitative microCT evaluation revealed that CMC-SF dressings had significantly larger micropores (102.4 ± 5.4 µm vs 62.5 ± 6.0 µm), higher porosity (91.9 ± 1.2% vs 75.3 ± 2.6%), and thinner pore walls (21.7 ± 2.1 µm vs 26.6 ± 1.2 µm) than CMC scaffolds (Figure 2G–I). Incubation for 24 h in phosphate-buffered saline (PBS), CMC dressings showed notable structural changes with ≈40% increase in micropore size, porosity rising to 93.5 ± 1.7% ($p < 0.05$), and thinner walls (20.6 ± 1.2 µm, $p < 0.05$), indicative of swelling and matrix relaxation. In contrast, CMC-SF dressings maintained a stable structure, attributed to the stabilizing effect of SF, which enhanced resistance to swelling and preserved scaffold integrity.

FTIR spectra showed characteristic peaks at 1640 and 1620 cm^{-1} in CMC-SF scaffolds (Figure S2A,B, Supporting Information), indicating the coexistence of α-helix and β-sheet structures in SF. CA acidification and CMC-SF interactions promoted a conformational shift toward hydrophobic β-sheets, further intensified by autoclave cross-linking, as seen by the enhanced 1620 cm^{-1} peak.[34–36] This agrees with previous studies reporting that autoclaving induces a stronger β-sheet formation than alternative methods such as ethanol treatment or air drying.[37] This transition is beneficial as β-sheet proportion influences scaffold stiffness, degradation, water absorption, and biological performance, including cell behavior and regeneration.[38–40]

Mechanical testing after 30 min in PBS (Table S1 and Figure S3, Supporting Information) demonstrated that CMC-SF dressings exhibited significantly higher elongation at break compared with CMC dressings ($p < 0.05$). These results confirm

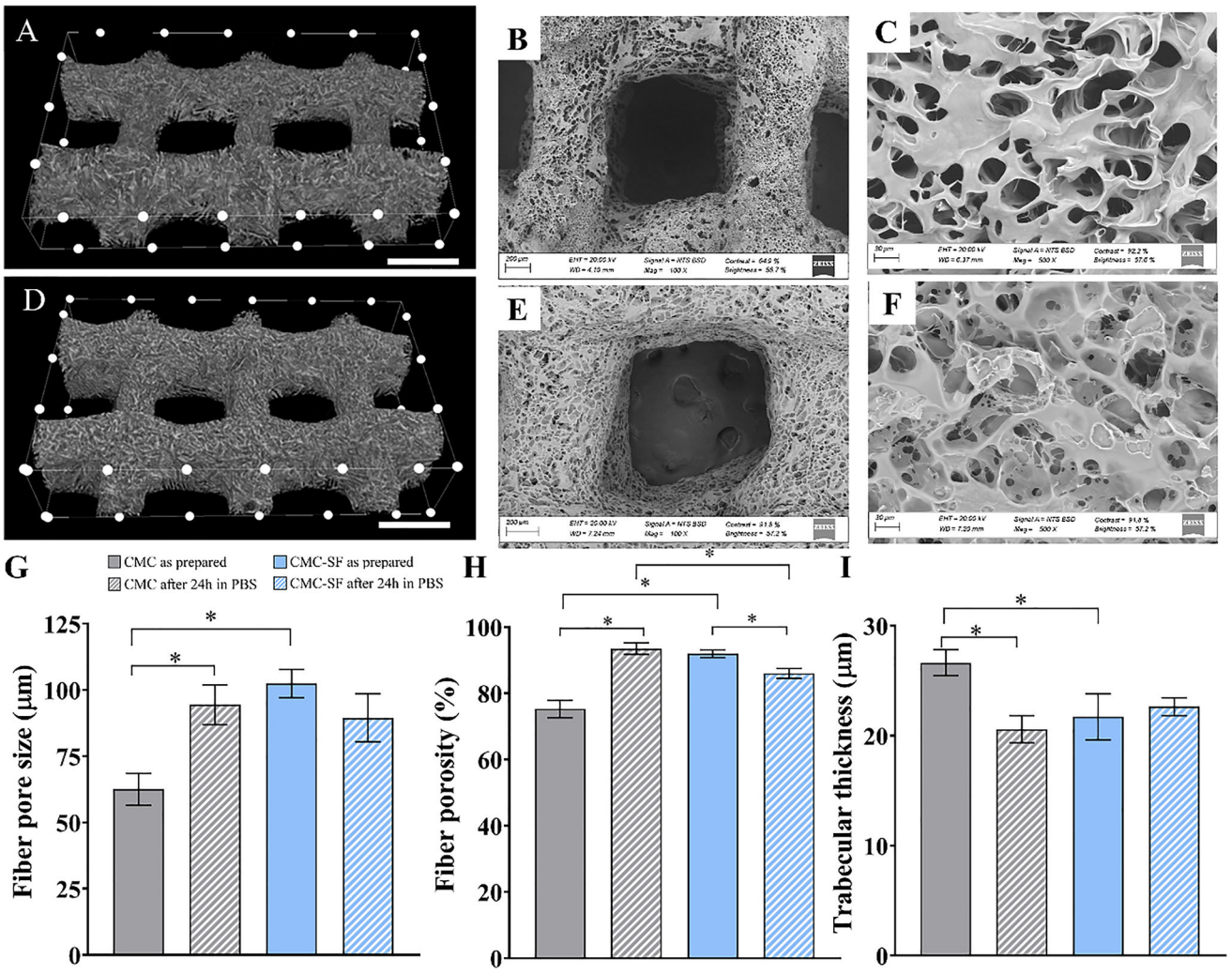

Figure 2. Structural characterization of CMC and CMC-SF scaffolds. Micro-CT reconstructions of CMC A) and CMC-SF D) dressings. Representative SEM micrographs of CMC B,C) and CMC-SF E,F) dressings. Quantitative analysis ($n = 6$) of fiber pore size G), fiber porosity H), and trabecular thickness, corresponding to the thickness of the walls of the fibers I), of CMC and CMC-SF freeze-dried dressings as prepared and after 24 h incubation in PBS. Scale bar is 500µm (A, D), 200 µm (B, E), and 30 µm (C, F). *Significant differences (ANOVA, $p < 0.05$).

that SF reinforcement enhances both mechanical strength and flexibility.[41,42] Notably, the mechanical properties of both dressings are within the range reported for other hydrogel-based wound dressings, underscoring their suitability for wound care applications.[43,44]

2.3. Swelling and Degradation Behavior

CMC and CMC-SF dressings were evaluated regarding their suitability for maintaining a moist wound environment. While simulated wound fluid would more closely mimic in vivo conditions, PBS was used for its simplicity and reproducibility, and results may vary slightly in a physiological environment. Both dressings rapidly absorbed PBS at 37 °C within the first hour, though CMC dressings showed lower swelling (≈500% at 2 days) and began degrading after 3 days (**Figure** 3A). However, CMC-SF dressings exhibited higher swelling (≈750% at 2 h) and retained structural integrity for at least 9 days, exceeding performance reported for CMC-SF-based films and electrospun mats.[45] In contrast, volumetric swelling (Figure 3B) showed that CMC dressings expanded more (≈117% at 1 h), while CMC-SF dressings presented a more controlled swelling (≈77% at 6 h), leading to more structural stability and minimizing the risk of significant deformation after application on the wound site. Furthermore, CMC-SF dressings retained more moisture in the early hours post-immersion ($p < 0.05$), equilibrating to ≈15% water content by 72 h (Figure 3C). This retention outperformed conventional PEG or alginate-based dressings, which typically dry out within 5–6 h.[46] A key limitation of dressings based on CMC or alginate, despite their widespread use in wound care, is their excessive swelling, which can compromise structural integrity, reduce patient comfort, and hinder the healing process by exerting pressure on the wound edges.[47–49] Incorporating SF, together with the cross-linking of CMC using CA, mitigated this issue, preserving shape and en-

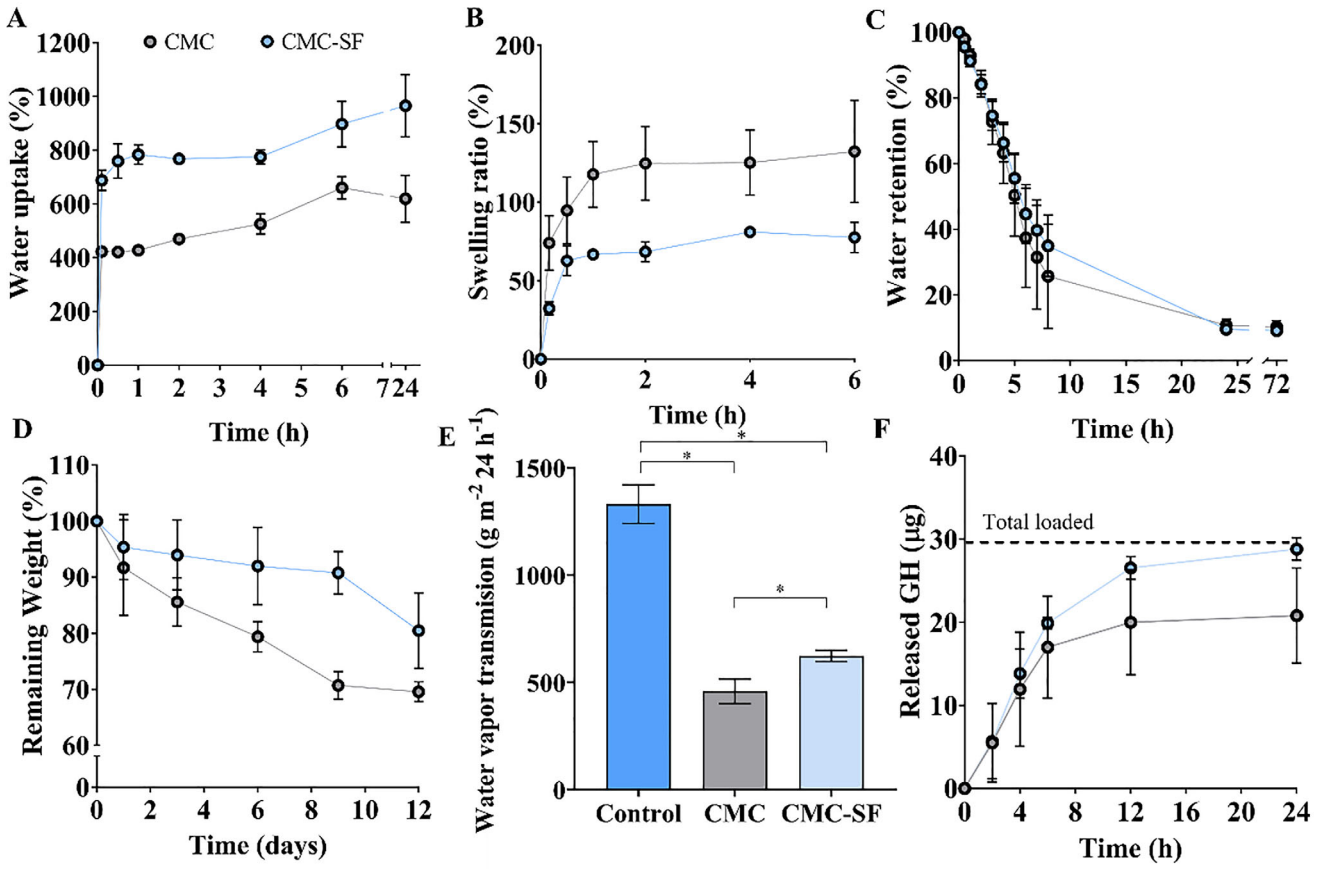

Figure 3. Swelling behavior of CMC and CMC-SF dressings, including A) solvent uptake in PBS; B) water retaining capacity, expressed as remaining water in the dressings during drying; C) volumetric swelling, which informs about the increase in the dimensions of the dressings during incubation in PBS; and D) erosion rate, corresponding to the weight loss during incubation in PBS. E) Water vapor transmission rate of the scaffolds. F) Growth hormone release profile in PBS. Data is shown as mean ± SD for $n = 5$. * means statistical differences ($p < 0.05$).

suring a stable fit over wounds while maintaining high moisture retention.[50]

Degradation profiles (Figure 3D) revealed that CMC-SF dressings retained over 80% of their initial mass after 12 days, whereas CMC dressings dropped to 70% and began to lose structural integrity, exhibiting fractures and increased brittleness. The addition of SF enhanced scaffold stability, potentially extending dressing wear time and reducing dressing changes. This observation aligns with previous reports exhibiting greater integrity of SF-based dressings compared with CMC dressings.[51,52]

The moisture permeability of CMC and CMC-SF dressings was assessed by measuring their water vapor transmission rate (WVTR) following European Standard EN 13726-2.[53] The results (Figure 3E) revealed that CMC-SF dressings had higher WVTR than CMC (622.2 ± 26.3 vs 457.5 ± 57.3 g m^{-2} 24 h^{-1}), attributed to their greater porosity. These values align with optimal WVTR ranges for natural polymer dressings, making CMC-SF more suitable for moderate-exudate wounds, while CMC is better for low-exudate applications.[54–56] Dressings displaying high WVTR (>5000 g m^{-2} 24 h^{-1}) can cause the wound bed to dry out quickly and become necrotic. Conversely, occlusive dressings with low WVTR (<300 g m^{-2} 24 h^{-1}) tend to accumulate exudate fluid, becoming more susceptible to infections.[55]

2.4. Growth Hormone Release

GH, a 22 kDa protein with an isoelectric point of ≈5.3, carries a net negative charge at physiological pH (7.4), as CMC and SF. This charge compatibility is important, since GH is known to undergo irreversible adsorption and conformational changes when exposed to cationic surfaces or alkaline conditions.[57] Its interaction with CMC and CMC-SF scaffolds likely involves weak hydrophobic forces, which may help maintain GH native conformation, as observed with other negatively charged hydrogels.[58] The GH concentration used was selected based on previous in vitro and in vivo data demonstrating its efficacy in stimulating cellular responses.[59] GH release was evaluated over 24 h in PBS at 37 °C using ELISA. Both dressings showed a rapid initial burst, releasing over 50% of GH within 2 h, followed by a slower release phase up to 24 h (Figure 3F). By 24 h, the release was nearly complete, indicating that GH adsorption onto the dressings was reversible, enabling efficient release into the wound bed. This profile is attributed to the high solubility of GH and its rapid diffusion from the dressing surface to the release medium. No significant differences were found between CMC and CMC-SF formulations. Rapid but controlled GH release can be particularly beneficial for diabetic ulcers, where growth factor levels are

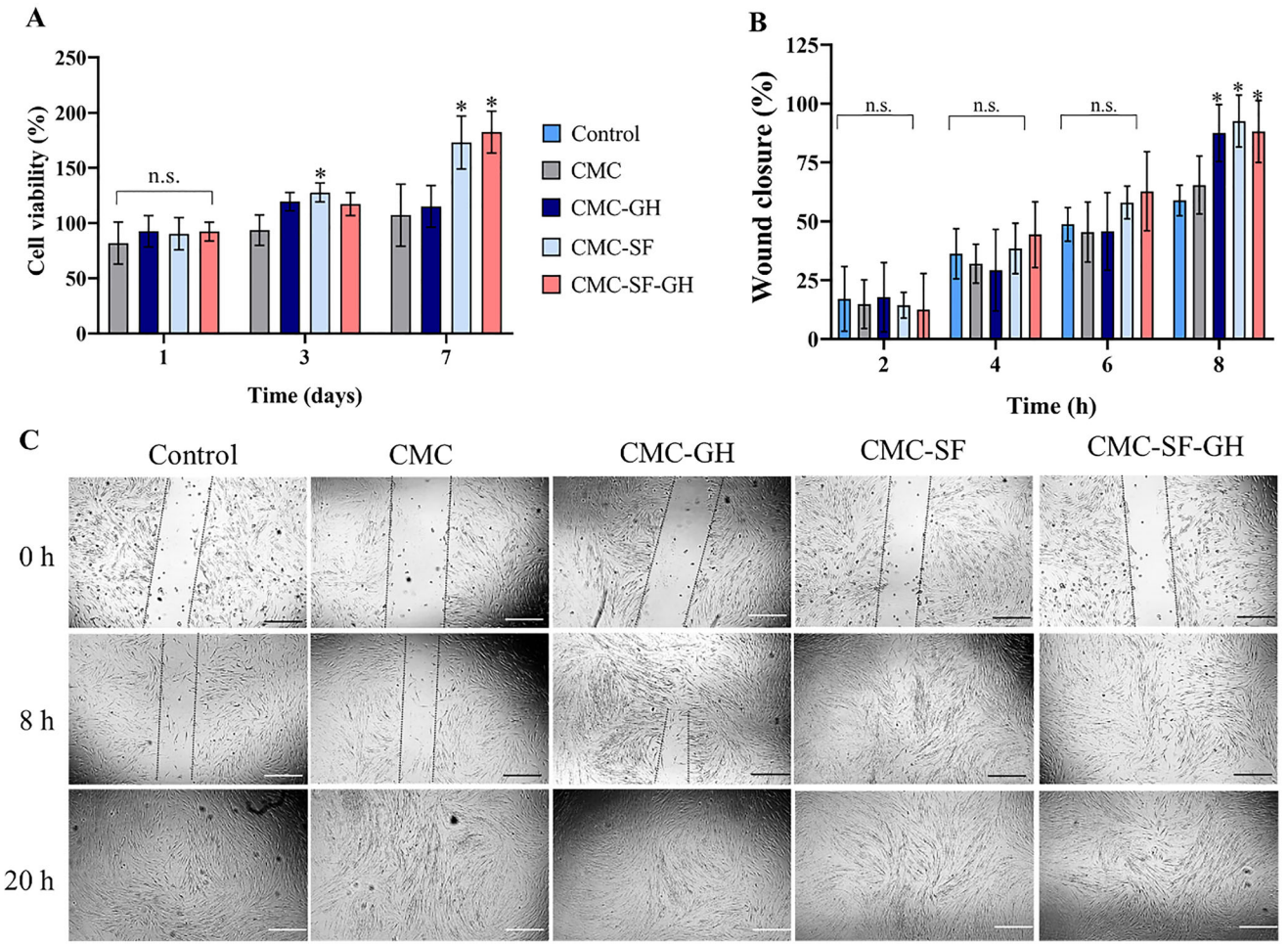

Figure 4. Results of HDF proliferation and migration in the presence of CMC and CMC-SF dressing released substances. A) Percentage of cell survival and proliferation in contact with byproducts after 7 days of culture. B) Quantification of the wound closure percentage for each condition. C) Pictures of the gap reduction in the scratch assay after 20 h of study. Scale bar is 500 µm. *significant differences ($p < 0.05$) with respect to the control (non-treated wells).

low. At the wound site, GH can promote vasodilation and activate several cellular pathways involved in proliferation and migration, like JAK2/STAT5 and SRC.[20,60]

2.5. In Vitro Evaluation of Cell Viability and Migration

Cell viability and proliferation were evaluated using three cell types relevant to wound healing: human dermal fibroblasts (HDFs), adipose-derived mesenchymal stem cells (adMSCs), and human keratinocytes (HaCaT). Cells were exposed to released substances from CMC and CMC-SF dressings, with or without GH. All formulations maintained viability above 70% at all time points, meeting ISO 10993–5 biocompatibility standards (**Figure** 4A; Figure S4, Supporting Information). In HDFs, SF-containing dressings significantly enhanced proliferation, particularly on days 3 and 7 (Figure 4A). adMSCs showed improved early viability with SF and GH, supporting their role in early-stage regeneration,[61] (Figure S4A, Supporting Information). HaCaT cells initially responded better to CMC and CMC-GH at 24 h, but by day 3, proliferation increased in SF-containing groups. By day 7, all groups showed comparable viability, confirming overall cytocompatibility. HaCaT cells, a spontaneously immortalized human keratinocyte line commonly used as a model for epidermal behavior due to their ability to mimic normal keratinocyte proliferation and differentiation,[62,63] initially responded better to CMC and CMC-GH at 24 h. However, by day 3, proliferation increased in SF-containing groups. By day 7, all groups showed comparable viability, confirming overall cytocompatibility (Figure S4B, Supporting Information).

A scratch assay using HDFs was conducted to assess the effect of released substances from CMC and CMC-SF dressings, both with and without GH, on cell migration. Released substances were obtained after 24 h of incubation in culture media at 37 °C and 5% CO_2. Scratch closure was evaluated up to 20 h by quantifying the remaining gap area (Figure 4B,C). Exposure to released substances from CMC-GH, CMC-SF, and CMC-SF-GH dressings resulted in significantly enhanced gap closure compared to the control and CMC-only groups. Nearly complete wound closure was observed in groups containing GH and SF, indicat-

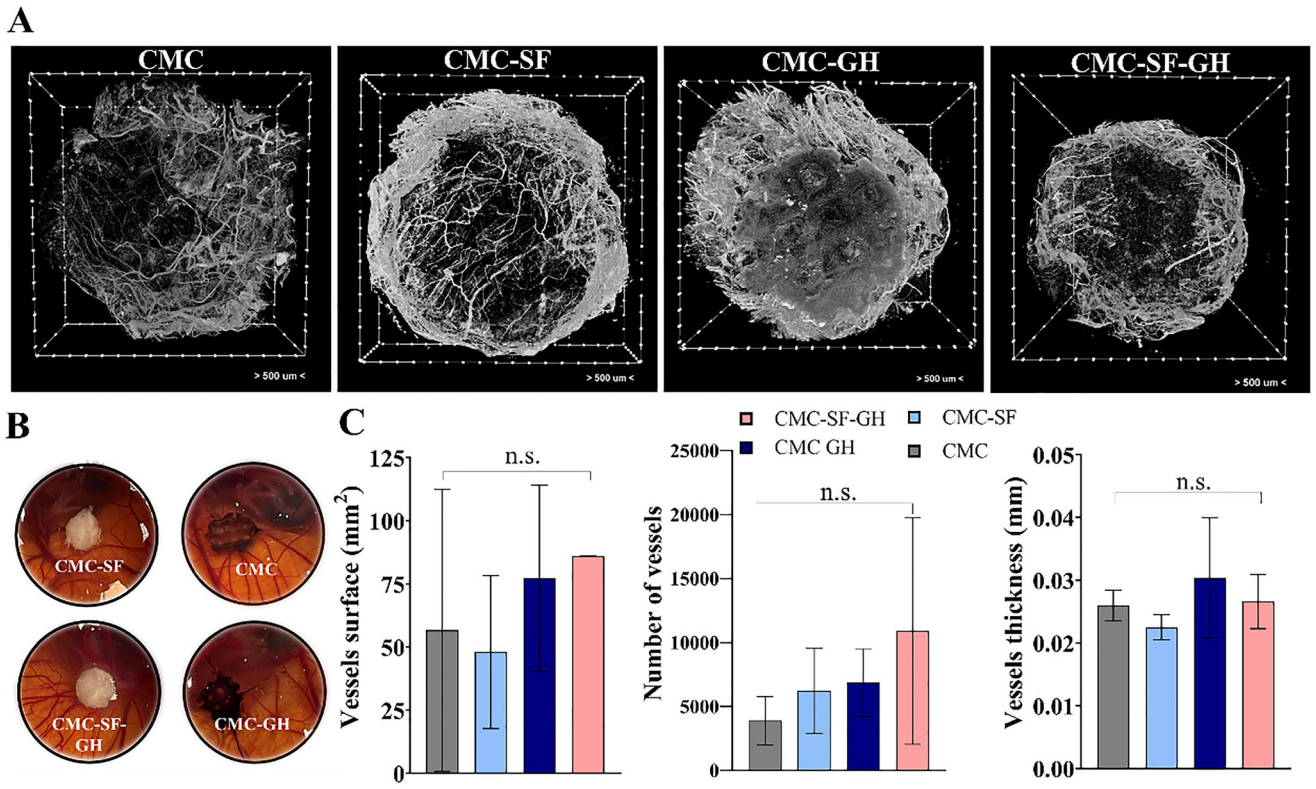

Figure 5. Results from the in ovo evaluation of CMC and CMC-SF dressings, both with and without GH loading: A) Micro-CT reconstructions of Lugol-stained blood vessels surrounding each dressing type (scale bar is 500 µm); B) Optical images of dressings implanted on the CAM, demonstrating nonhaemolytic effects and compatibility with CAM development; C) Quantitative analysis of Micro-CT-scanned CAMs assessing vessel surface area, number of vessels, and thickness.

ing enhanced fibroblast migration. These findings are consistent with previous reports demonstrating the pro-migratory effects of GH and SF.[22,64] Notably, these results underscore the potential of the developed dressings as customizable platforms for localized GH delivery, promoting wound healing not only through sustained release but also by actively facilitating cell migration at the injury site.[24]

2.6. Evaluation of Hemostatic Properties

The hemostatic properties of CMC and CMC-SF dressings were assessed to determine their ability to promote early clot formation as an essential step in wound healing. SEM analysis revealed that both dressings supported the adhesion of RBCs and activated platelets, identifiable by their spread morphology and pseudopodia, indicative of early clot formation (Figure S5A,B, Supporting Information). Upon blood contact, both CMC and CMC-SF samples retained blood cells without causing RBC lysis, demonstrating good hemocompatibility (Figure S5C,D, Supporting Information). Consistent with prior findings on polysaccharide-based materials, the polyelectrolyte nature of CMC and SF likely facilitated electrostatic interactions with blood components.[65] Notably, CMC-SF dressings promoted the formation of a fibrin network within their porous structure (Figure S5C, Supporting Information), suggesting activation of the coagulation cascade.[65] In contrast, CMC dressings did not exhibit visible signs of fibrin formation.

Clotting efficiency was further evaluated by measuring the blood coagulation index (BCI), which quantifies haemoglobin released from lysed red blood cells, where lower BCI values indicate higher clotting efficacy. CMC dressings exhibited BCI values close to 1, similar to the negative control, suggesting limited clotting activity. Conversely, CMC-SF dressings showed a significantly reduced BCI (0.63), confirming their enhanced capacity to promote coagulation upon contact with blood (Figure S5E, Supporting Information).

2.7. *In Ovo* Evaluation of Tissue Integration and Angiogenesis

The in ovo chorioallantoic membrane (CAM) model is a valuable, ethical alternative to traditional animal testing for studying angiogenesis.[66–68] Aligned with the 3Rs principle, it reduces animal use while allowing real-time observation of early biological responses that are often challenging to capture in conventional in vivo models.[69] Macroscopic examination of CMC and CMC-SF dressings showed no significant tissue invasion or cytotoxicity after 12 days, with blood vessels surrounding but not infiltrating them (**Figure 5B**). Micro-CT reconstructions further demonstrated the preservation of tissue architecture (Figure 5A). Quantitative analysis revealed no significant differences between

CMC and CMC-SF dressings in vessel volume, surface area, or diameter (Figure 5C). Importantly, the dressings remained non-integrative, facilitating easy removal without damaging the surrounding tissue. This is an advantage for clinical wound care, where atraumatic dressing changes are critical for continuous healing.

2.8. In Vivo Evaluation in Diabetic, Ischemic Wound Model

The regenerative potential of CMC and CMC-SF dressings was evaluated using an ischemic wound model in diabetic rats, which closely replicates key characteristics of diabetic ulcers, including impaired vascularization and compromised nerve function.[25,70] From the initial number, five rats deceased following diabetes induction with streptozotocin, four were excluded due to excessive edema or dehiscence in the ischemic area, and one was excluded for showing signs of illness (underweight and infection). Daily wound assessments (**Figure 6A**) were conducted to monitor closure progression and signs of infection or inflammation. By day 14, all wounds exhibited visible healing (Figure 6B). Although no statistically significant differences in wound closure rates were observed among the treatment groups at any time point, a consistent visual trend suggested that wounds treated with SF-containing dressings (CMC-SF and CMC-SF-GH) tended to close more rapidly and extensively than those in the control group.

Hematoxylin-eosin (H&E) staining (Figure 6C) demonstrated the presence of granulation tissue in all groups by day 7, although the tissue architecture appeared disorganized across treatments at this early stage. By day 14, more mature and organized tissue structures were observed, particularly in the CMC-GH, CMC-SF, and CMC-SF-GH groups. These groups exhibited well-distributed hair follicles and blood vessels, and granulation tissue had largely been replaced by normal dermal tissue, indicating enhanced remodeling and regenerative capacity. In contrast, the control group showed incomplete re-epithelialization and a sparse distribution of hair follicles within the wound area at the same time point. Notably, wounds treated with GH-containing dressings displayed a thicker epidermal layer as early as day 7 post-surgery, compared to both the control and the groups treated with CMC or CMC-SF alone, suggesting an accelerated epithelial response facilitated by GH.

Immunohistochemical analysis further supported these findings. CD31 staining demonstrated significantly increased blood vessel density in wounds treated with CMC-GH, CMC-SF, and CMC-SF-GH dressings (Figure 6D; Figure S6, Supporting Information), highlighting the angiogenic effects of both SF and GH, which are critical factors in counteracting ischemia-related healing impairments in diabetes. Additionally, PCNA staining revealed elevated levels of cellular proliferation in all SF- and GH-containing treatments, with the highest proliferation observed in the CMC-SF-GH group ($p < 0.05$ vs all other groups) (Figure 6E; Figure S7, Supporting Information), which suggests a synergistic effect of SF and GH in promoting wound healing at both the cellular and vascular levels. It is worth noting that the application of dressings may have mechanically limited wound contraction, the primary healing mechanism in rodents, thereby reducing the apparent closure rate compared to untreated wounds. Despite this, histological analysis revealed marked differences in tissue regeneration quality between groups.

To further explore the molecular mechanisms underlying the biological response to the different dressings, a comparative proteomic analysis was conducted. Venn diagrams of the proteins identified at days 5 and 14 illustrated both shared and unique protein expression profiles across the treatment groups (**Figure 7A**). On day 5, 241–259 proteins were commonly expressed among all groups, reflecting core wound healing processes that are independent of treatment. However, distinct subsets of proteins were identified for CMC-GH (17 unique proteins) and CMC-SF-GH (41 unique proteins), suggesting that the incorporation of SF and GH activates specific molecular pathways. By day 14, the number of shared proteins increased significantly (333–367), indicating that as the healing process advanced and the initial inflammation decreased, the molecular profiles of the treatments began to converge. GH-containing formulations maintained distinct protein expression patterns, indicating an early activation of regenerative pathways. The intermediate profile observed in the CMC-SF group further emphasizes the role of the biomaterial composition in modulating cellular responses and influencing the wound healing process.

To elucidate the molecular mechanisms underpinning the wound healing response to CMC- and CMC-SF-based dressings, a quantitative proteomic analysis using the SWATH-MS method was performed on tissue samples collected at days 5 and 14 post-treatment. Volcano plots (Figure 7B) and heatmaps (**Figure 8**) revealed distinct protein expression profiles across treatment groups, particularly in formulations containing SF and GH, compared to untreated controls. Proteomic profiling demonstrated a consistent upregulation of proteins involved in extracellular matrix (ECM) remodeling, angiogenesis, and immune modulation in treated wounds (**Figure 9A**). On day 5, CMC-treated wounds showed elevated levels of COL1A1, indicative of early collagen synthesis, while COL1A2 was upregulated at day 14, suggesting sustained matrix deposition and tissue regeneration.[71] In addition, the upregulation of CUL3 in CMC-treated wounds on day 14, and its earlier presence in CMC-SF-GH, points to enhanced cellular proliferation and reduced fibrotic potential.[72]

Immune-related proteins were also prominently elevated. LRP1, SERPINE1, and POSTN are key mediators of inflammation resolution and tissue repair and were significantly upregulated in GH-containing groups (Figure 9B), aligning with prior studies on diabetic wound healing.[73,74] Notably, immunoglobulin proteins such as IGHG1 and IGG2C were upregulated across all CMC-based treatments by day 14, suggesting a robust humoral immune response. This may reflect enhanced immune surveillance and clearance of cellular debris, critical for transitioning from inflammation to tissue repair.[75]

In CMC-SF-treated wounds, FIBG (fibroblast growth factor-binding protein) was upregulated as early as day 5, a pattern also observed in CMC-GH-treated wounds at early timepoints. This early upregulation underscores FIBG's role in promoting fibroblast and endothelial cell proliferation.[76] Additionally, FIBG is strongly associated with activation of the IGF signaling pathway, indicating an early effect of GH on the tissue (Figure 9C). Similarly, FABP5, associated with dermal regeneration, was elevated at day 14 in the CMC-SF group, reinforcing the regenerative potential of the dressings.[30] GH-treated wounds also exhibited

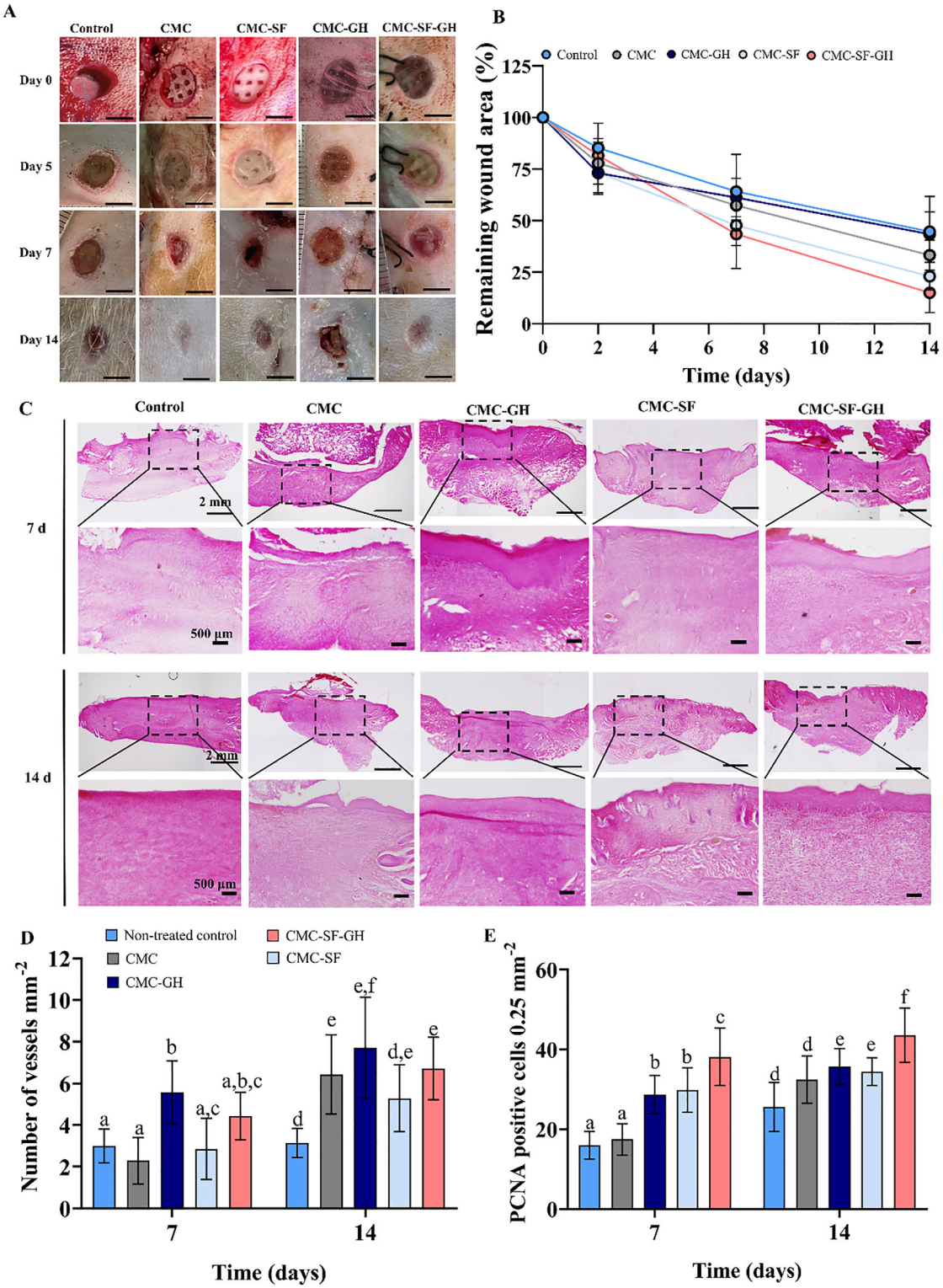

Figure 6. A) Optical pictures of the wounds treated with the different dressings at different timepoints of the study. Scale bar is 5 mm. B) Evaluation of wound closure expressed in remaining area (%) compared to the initial gap at each time point. C) Histological analysis of wounds treated with CMC, CMC-SF (both loaded and non-loaded with GH), and untreated control groups at days 7 and 14 post-surgery. D) Quantification of microvessel density in wound sections following treatment with CMC or CMC-SF dressings (with and without GH), compared to untreated controls, at days 7 and 14. E) Quantification of PCNA-positive cell density in wounds treated as for the CD31 and untreated controls on days 7 and 14. Untreated wounds served as the control group. Different letters indicate statistically significant differences between groups at each time point ($p < 0.05$; $n = 7$).

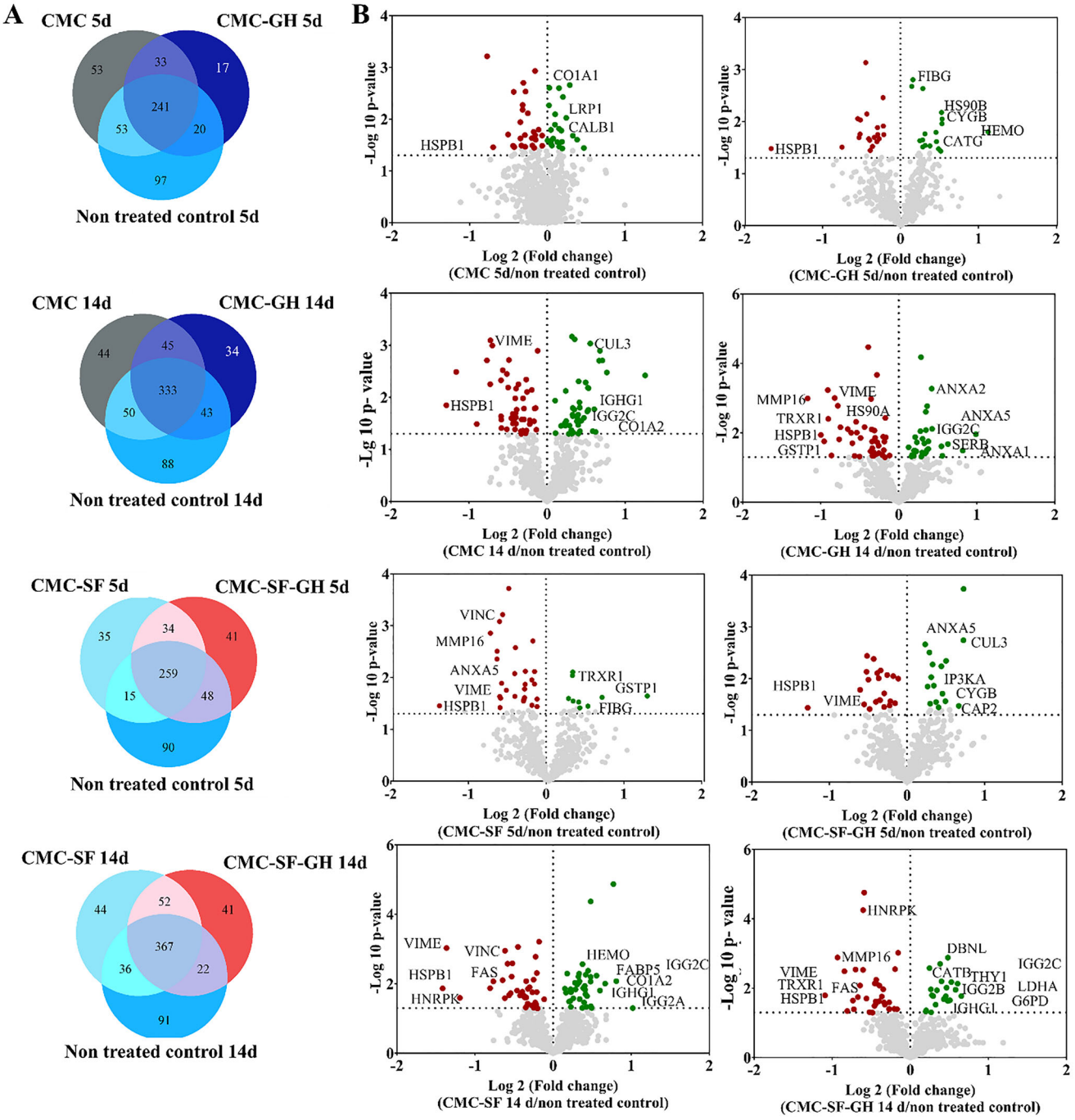

Figure 7. Proteomic profile of expressed proteins in wounds with different treatments. A) Venn diagrams illustrating the number of shared and unique proteins identified across three different treatment groups at each time point. B) Volcano plots displaying differentially expressed proteins between two conditions by SWATH-MS analysis, representing the expression changes in the first-mentioned treatment relative to the second. Significantly regulated proteins ($p < 0.05$) are plotted with $\log_2$ fold change on the *x*-axis. Proteins in gray showed no significant change, while green and red dots indicate proteins that were significantly upregulated or downregulated, respectively, in the treated group. Selected key proteins are annotated with their respective identifiers.

increased expression of antioxidant proteins such as CATG and CYGB, suggesting improved oxidative stress management and tissue remodeling. These molecular signatures correlate with histological observations of enhanced vascularization and cellular proliferation in GH- and SF-treated wounds.[77]

Annexin family proteins, including AnxA1, AnxA2, and AnxA5, were differentially expressed in response to treatment. These proteins are known for their anti-inflammatory, membrane-stabilizing, and pro-fibrinolytic roles in wound healing.[78] On day 14, CMC-GH-treated wounds showed strong

Figure 8. Heatmaps representing the significantly different proteins ($p < 0.05$) between conditions with and without SF and GH. Green boxes mean upregulation, while pink boxes mean downregulation, and white means close to 0-fold change. Right lines indicate clusters attending to different proteins (regarding the rows).

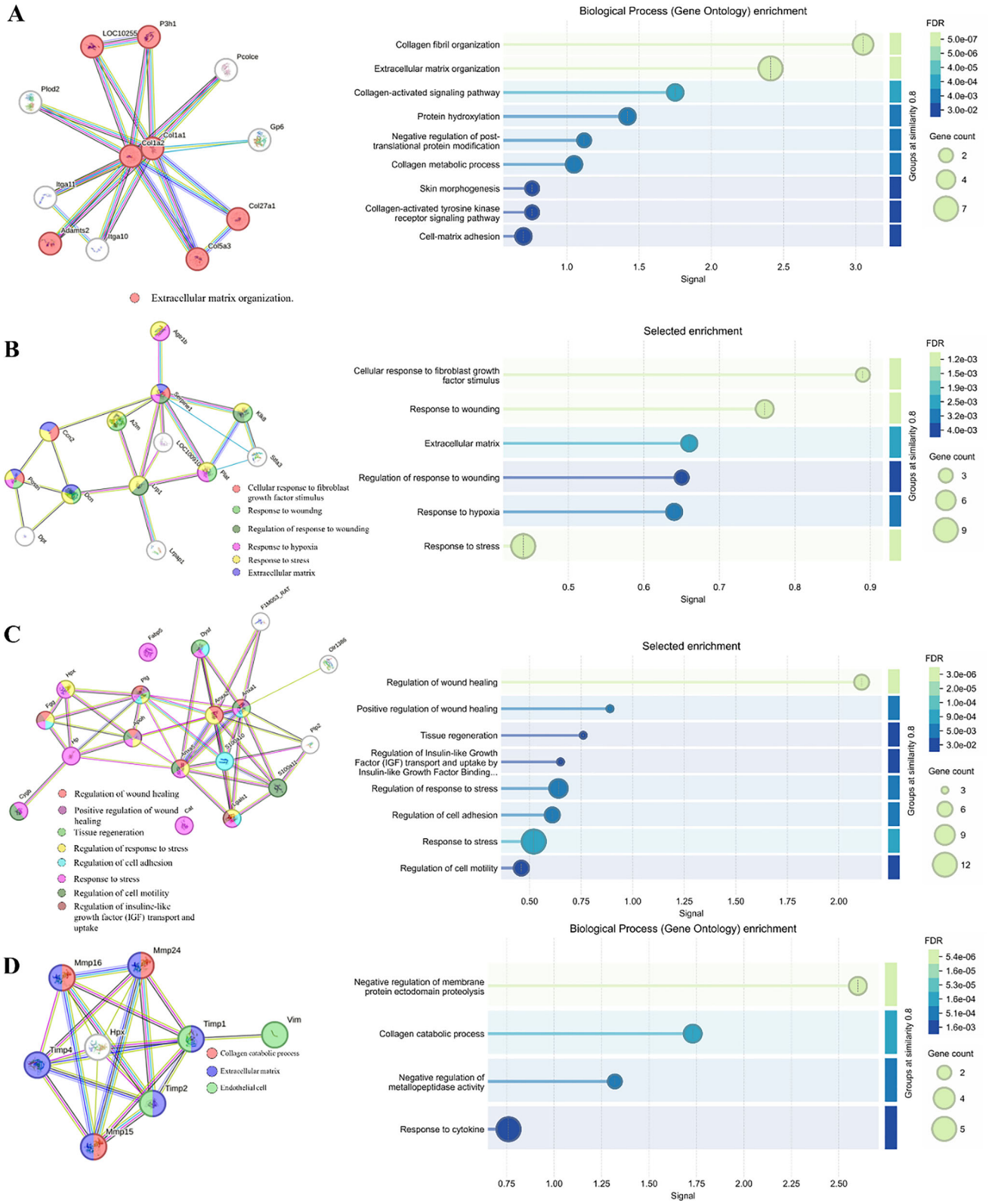

Figure 9. Representative protein interactions (confidence > 0.700) of different processes presented in the treated wounds, and functional analysis of the enriched pathways for: A) ECM formation; B) Inflammatory and immune response; C) Regeneration-related pathways; and D) Inhibition of excessive ECM deposition.

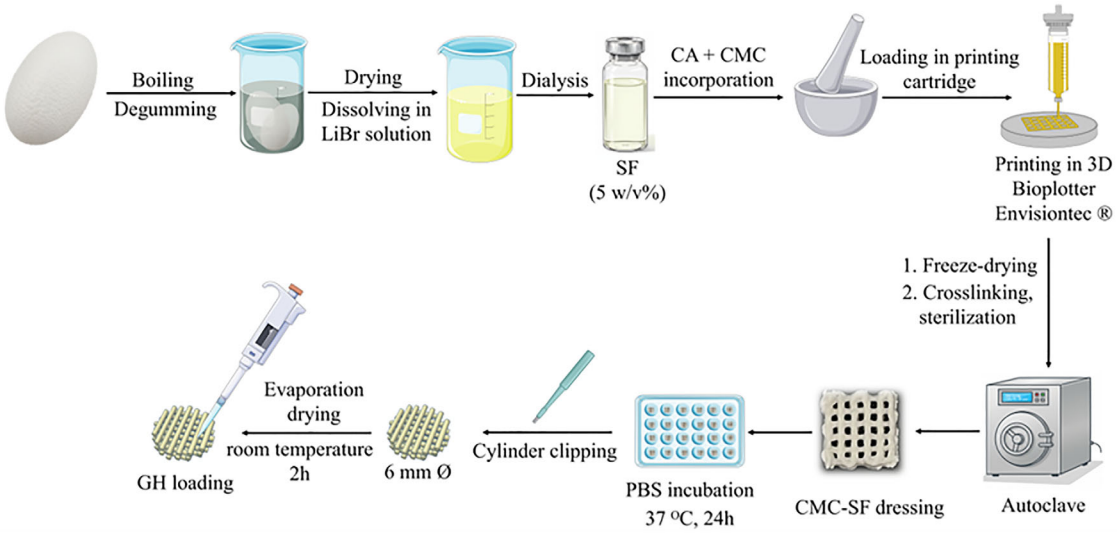

Figure 10. Workflow for preparation of CMC-SF dressings and their post-treatment for sterilization, cross-linking, and GH loading. CMC dressings were prepared similarly, but using distilled water instead of the SF solution.

upregulation of all three annexins, indicating active resolution of inflammation and protection against thrombosis. AnxA5 was also elevated in CMC-SF-GH on day 5, whereas its downregulation in CMC-SF alone suggests GH is a key driver of annexin-mediated responses. Temporal regulation was evident, with AnxA4 downregulated in CMC-GH on day 5 and AnxA1 reduced on day 14, reflecting stage-specific roles in healing. The HEMO protein, involved in hypoxia response and interferon-γ signaling, was upregulated in CMC-GH (day 5) and CMC-SF (day 14), suggesting these dressings support immune-mediated repair under ischemic conditions.[79]

Proteins associated with chronic inflammation and excessive ECM turnover were downregulated in treated wounds, indicating a more regulated healing environment (Figure 9D). MMP16, a matrix metalloproteinase linked to ECM degradation, was suppressed in CMC-SF on day 5, consistent with reduced tissue breakdown.[80] Although transiently elevated in GH-treated wounds at day 5, MMP16 was significantly downregulated by day 14, suggesting an initial remodeling phase followed by resolution. Similarly, other proteins such as VIME (vimentin) and HSPB1, both linked to fibrosis and chronic stress responses, were downregulated. Their reduced expression in GH- and SF-treated wounds may indicate improved tissue organization and a shift toward homeostasis.[81]

3. Conclusion

CMC-SF dressings developed in this study combined excellent printability, structural integrity, and biological performance. Incorporation of silk fibroin enhanced mechanical strength, structural stability, and microporosity compared to CMC-only dressings. Both dressings effectively absorbed and retained moisture; however, CMC-SF exhibited reduced volumetric swelling and slower degradation, which are key attributes for maintaining a moist wound environment without compromising conformability or necessitating frequent replacement. The *in ovo* assay confirmed the biocompatibility and non-integrative nature of the dressings, enabling safe removal without tissue damage. The ischemic wound model offered a clinically relevant platform to evaluate therapeutic efficacy. Results indicated that the combination of SF and GH synergistically enhanced tissue regeneration, reduced fibrotic tissue formation, and promoted the restoration of tissue homeostasis and vascularization. These findings were corroborated by histological, immunohistochemical, and proteomic analyses.

The developed CMC-SF-GH wound dressings represent a significant advancement over conventional topical treatments, which are primarily passive in function—limited to exudate management or infection control. In contrast, the proposed approach introduces a bioactive delivery system capable of actively modulating the biological response of injured tissue. Furthermore, the integration of 3D printing allows for the customization of dressings, supporting the development of precise, patient-specific therapies tailored to the unique characteristics of each wound and clinical condition, aligning with the broader goals of personalized medicine.

4. Experimental Section

Materials: Sodium carboxymethyl cellulose (CMC, 395 kDa, degree of substitution (DS) 0.9, viscosity 2% NF 2960 cPs, 8.8% Na) was from Ashland (Blanose 9M31F PH; Wilmington, DE, USA). Citric acid anhydrous (CA) was from Panreac (Barcelona, Spain). MEM-α (Minimum Essential Medium-α), DMEM (Dulbecco's Modified Eagle Medium), RPMI 1640 (Gibco Cat. no. 11875093), fetal bovine serum (FBS), penicillin/streptomycin 100x solution, TrypIE, AlamarBlue cell viability reagent, and Dulbecco's Phosphate Buffered Saline (DPBS) were from ThermoFisher Sci (Waltham, MA, USA). GH (Humatrope 6 mg) was from Eli Lilly (Basingstoke, UK). Human GH ELISA Kit (RAB0206) and streptozotocin (CAS 18883-66-4) were from Sigma–Aldrich, (Saint Louis, MO, USA). Ultrapure water (resistivity > 18.2 MΩ cm; Milli-Q, Millipore Ibérica, Madrid, Spain) was obtained by reverse osmosis. Human dermal fibroblasts (HDF, P10858) were from Innoprot (Derio, Spain). Adipose-derived mesenchymal stem cells (adMSCs, passage 10; PCS-500-011) and human

Table 1. Composition of CMC and CMC-SF inks tested as candidates for ink development.

Ink code	CMC (w/v%)	SF (w/v%)	CA (w/w_{CMC}%)
CMC_{15}	15	0	20
CMC_{20}	20	0	20
CMC_5-SF_5	5	5	20
CMC_6-SF_5	6	5	20
CMC_7-SF_5	7	5	20
CMC_{10}-SF_5	10	5	20

keratinocytes (HaCaT, passage 7; PCS-200-011) were from ATCC (Manassas, VA, USA). Aqueous SF solutions were prepared under GMP conditions at IMIDA (Murcia, Spain) following a robust standard procedure previously described, and batch-to-batch consistency was confirmed by FTIR and SDS-PAGE.[82]

Ink Preparation and 3D Printing: The workflow for ink preparation and 3D printing of wound dressings is illustrated in **Figure 10**. CMC and CMC-SF inks were prepared using the components listed in **Table 1**. For CMC-SF inks, an SF solution was adjusted to pH 8 (dropwise addition of 0.1N NaOH), heated to 37 °C, and combined with CA (20 w/w% relative to CMC) using a mortar and pestle. CMC powder was gradually added and mixed until a uniform ink was obtained. CMC inks were prepared by dissolving CA (20 w/w_{CMC}%) in water, followed by the addition of CMC at 15% or 20 w/v%.

The rheological properties of the freshly prepared inks were analyzed using a MCR 302 rheometer (Anton Paar; Graz, Austria) with a Peltier module and an aluminum plate (15 mm diameter, 1 mm gap, 20 °C). G′ (storage modulus) and G″ (loss modulus) were recorded applying five cycles, simulating the shear conditions experimented by the inks during the extrusion printing: 1) 0.5% shear strain at 1 Hz for 300 s; 2) 100% shear strain at 1 Hz for 120 s; 3) 0.5% shear strain at 1 Hz for 300 s; 4) 100% shear strain at 1 Hz for 120 s; and 5) 0.5% shear strain at 1 Hz for 300 s.[83] Additionally, ink printability and resolution were tested. Inks were printed using a woodpile pattern consisting of three zig-zag layers, based on a 10 × 10 mm square 3D model. Printing pressure and speed were individually adjusted for each ink to produce filaments with consistent dimensions across all conditions. Images were taken using the camera coupled to the printer and analyzed using ImageJ (NIH, Bethesda, MD) for pore shape and fiber size.

Wound dressings were fabricated layer-by-layer using a Bioplotter Manufacturer 3D printer (EnvisionTEC GmbH; Gladbeck, Germany) equipped with a 22G nozzle. For CMC-SF inks, the extrusion parameters were set to 1.9 bar pressure and 6 mm s^{-1} printing speed, for CMC inks, 3.3 bar and 3 mm s^{-1} were used. Cubic models (10 × 10 × 5 mm) were designed in SketchUp (Trimble Inc., Westminster, CO, USA) and printed onto glass slides with a woodpile lattice pattern and 1.8 mm line spacing. To prevent fiber collapse, the printing platform was maintained at 10 °C. After printing, the dressings were immediately frozen and freeze-dried for 24 h. Cross-linking using CA and sterilization were performed simultaneously by autoclaving at 121 °C for 20 min. The dressings were stored at room temperature in sealed vials until use. Prior to experiments, dressings were cut into 6 mm diameter discs using a biopsy punch and individually incubated in 2 mL of DPBS at 37 °C for 24 h to remove unreacted CA. Finally, the dressings were air-dried under sterile conditions in a laminar flow hood for 2 h.

Dressing Characterization: Freeze-dried CMC-SF and CMC dressings, after cross-linking/sterilization, were sputter-coated with gold-palladium and observed using an EVO LS 15 SEM (Zeiss; Oberkochen, Germany). The structure and pore distribution of the dressings ($n = 6$) were analyzed using a Skyscan 1272 X-ray microCT (Bruker; Kontich, Belgium). Projections were acquired using a 5 µm resolution and no filter at 50 kV and 200 mA, and subsequently reconstructed and volume rendered using NRecon and CTVox software (Bruker; Kontich, Belgium), respectively. Structure analysis, including pore size distribution, porosity, fiber thickness, and interconnectivity, was carried out using CTAn software (Bruker; Kontich, Belgium).

Infrared spectra of SF stock solution and printed dressings before and after cross-linking were recorded with an ATR-FTIR Varian 670-IR (Varian Inc.; Palo Alto, CA) within the 400–4000 cm^{-1} range at a resolution of 2 cm^{-1}.

Freeze-dried samples were incubated in PBS at 37 °C, and water absorption, dimensional swelling, moisture loss over time, and material erosion were quantified at predetermined timepoints to assess hydration behavior and structural stability. Full experimental details, equations, and protocols are provided in Section S2.1 (Supporting Information). To evaluate the WVTR, dressings ($n = 5$) were individually placed over water-filled cylindrical tubes (1.5 cm diameter, 8 mL water), sealed, and incubated at 37 °C and 20% relative humidity for 24 h. Control tubes without dressings were also tested. Moisture loss was determined by weighing the tubes before and after incubation.

The tensile strength of the printed dressings was measured using a texture analyzer (TA.XT Plus, Stable Micro Systems, Surrey, UK) fitted with a 5 kg load cell (UNE-EN 13726-4 standard). CMC-SF and CMC dressings were printed in 30 × 10 × 2 mm rectangular prisms, incubated in PBS for 30 min to simulate exudate absorption, and stretched until they broke at a crosshead speed of 0.1 mm s^{-1} with a 10 mm gap. Tensile strength, Young´s modulus, and elongation at break were calculated from the resulting stress–strain curves.

Growth Hormone Loading and Release: CMC and CMC-SF dressings (6 mm diameter) were placed in 24-well plates and loaded with GH by applying 30 µg of GH (3 mg mL^{-1}) onto each dressing. After absorption, the dressings ($n = 5$ per group) were individually incubated in 1 mL of DPBS at 37 °C. At set timepoints (2, 4, 6, 12, and 24 h), 0.5 mL of the release medium was collected and replaced with fresh DPBS. Collected volumes were transferred to 1.5 mL LoBind microcentrifuge tubes (Eppendorf; Hamburg, Germany) and stored at −80 °C until analysis. GH release was quantified using a Human GH ELISA Kit (Sigma–Aldrich, Saint Louis, MO, USA) according to the manufacturer´s instructions.

Cell Viability and Migration: HDFs (P10858, passage 4) were cultured in DMEM supplemented with 10% FBS and 1% antibiotic/antimycotic at 37 °C and 5% CO_2. At ≈80% confluency, cells were trypsinized and seeded in 48-well plates at 3 × 10^4 cells per well. CMC and CMC-SF dressings (6 mm), with or without GH loading (50 ng mL^{-1}, 150 mIU L^{-1}), were immersed in 0.5 mL of supplemented DMEM. After 24 h, the HDF culture medium was replaced with the lixiviates, and cell proliferation was assessed on days 1, 3, and 7 using the AlamarBlue assay (Invitrogen). Fluorescence (excitation 540 nm, emission 580 nm) was measured with a spectrophotometer. Cell viability of adMSC and HaCaT keratinocytes was also tested with the released substances (Section S2.2, Supporting Information).

A scratch assay was conducted with HDF to evaluate cell migration. Upon reaching confluence, a 500 µm full-thickness scratch was created at the center of the monolayer using a 10 µL pipette tip. The wells were then washed three times with PBS to remove cellular debris, after which 0.5 mL of either the test-released substances or complete culture medium (control) was added. The assay was carried out for a total duration of 20 h. Images of the scratch were captured using a CKX53 inverted microscope equipped with an EP50 digital camera (Olympus, Tokyo, Japan) and analyzed with ImageJ software (NIH, Bethesda, MD). Wound closure was quantified by measuring the reduction in gap distance over time relative to the initial width.

Hemocompatibility Evaluation: All procedures involving human blood samples were conducted in accordance with ethical guidelines and regulations. Ethical approval was obtained from the Galician Research Ethics Committee (registry code: CEI2025/160). Written informed consent was obtained from healthy adult volunteers, in compliance with the Declaration of Helsinki. Hemocompatibility of CMC and CMC-SF dressings (6 mm, $n = 3$) was assessed using SEM for blood cell adhesion and measuring the BCI.[84,85]

To evaluate RBC and platelet adhesion, 100 µL of whole blood was added to the dressings, incubated at 37 °C for 30 min, rinsed three times

with distilled water, frozen at –80 °C, and freeze-dried for 12 h. SEM imaging was performed after gold–palladium sputter coating using an EVO LS 15 microscope (Zeiss; Oberkochen, Germany).

For BCI analysis, dressings were placed in 12-well plates and prewarmed at 37 °C for 10 min. Then, 200 µL of whole blood and 20 µL of 0.2 M $CaCl_2$ were added to each well. After a 10-min incubation at 37 °C and 100 rpm, 2.5 mL of distilled water was added to lyse free RBCs. The absorbance at 540 nm was measured using a FLUOstar OPTIMA plate reader (BMG Labtech), and BCI was calculated based on the ratio of sample absorbance (As) to fully lysed blood absorbance (A0) using Equation (1):

$$BCI = \frac{A_s}{A_0} \quad (1)$$

In ovo Evaluation of Tissue Integration and Angiogenesis: The integration and vascular response of CMC and CMC-SF dressings, with or without GH, were evaluated using the CAM assay in fertilized chicken eggs (Coren, San Cibrao das Viñas, Ourense, Spain).[86] On embryonic day 8, dressings (6 mm, $n = 5$) were placed on the CAM and incubated until day 12. CAMs were fixed with 4% paraformaldehyde for 4 h, and the CAM tissue around each dressing (≈25 mm in diameter, centered on the scaffold) was excised using a scalpel, and then stained with 0.5% iodine solution protected from light. Following 2 h staining, samples were washed three times with DPBS and freeze-dried.

Neovascularization was assessed via micro-CT (Skyscan 1272, Bruker; Kontich, Belgium). Imaging was performed at 50 kV and 200 µA, with a 4 µm pixel size, 350 ms exposure time, 0.4 mm rotation step, and no filter. The scan resolution was 4032 × 2688 pixels. Image reconstruction was performed with NRecon software (Bruker), using a histogram range of 0–0.1. CTAn software (Bruker) was used to quantify the surface, thickness, and volume of blood vessels formed in the CAM surrounding the dressing.

In Vivo Evaluation: The in vivo test protocol was approved by the Health Research Institute of Santiago de Compostela (IDIS) Bioethics Committee for Animal Studies (protocol 15012/2024/010) and conducted in accordance with the European regulation on care and use of animals in experimental procedures and ARRIVE guidelines.

CMC and CMC-SF dressings, with or without GH (30 µg), were tested in a diabetic ischemic ulcer wound model in rats (30 animals, male, Sprague-Dawley, 200–215 g housed at 23 ± 2 °C under a 12 h light/dark cycle and ad libitum feeding). Diabetes was induced with streptozotocin (i.p. injection of 60 mg kg^{-1}; 0.2–0.5 mL volume based on body weight) and blood glucose levels were monitored for 7 days. After confirming diabetic symptoms (glucose levels exceeding 220 mg dL^{-1}, polyuria, polydipsia, and polyphagia), the animals were housed for 6 weeks to develop a delayed healing phenotype. Surgical procedures were performed under continuous isoflurane inhalation in the animals: 5% for induction and 2.5% for maintained anesthesia. The dorsal skin was shaved using an electric trimmer, followed by depilatory cream. Ischemic wounds were then created following a previously described and adapted protocol.[70] Briefly, a 10.5 × 3 cm rectangle was marked centrally on the dorsal skin. Four full-thickness wounds were created using a 6 mm biopsy punch. Then, a bipedicle flap was raised along the outlined rectangle with a sterile scalpel, and the panniculus carnosus fascia was carefully separated from the underlying muscles using iris scissors, ensuring fascia integrity. A medical-grade silicone sheet (TecnoProducts, Barcelona, Spain), previously cut to fit the flap dimensions, was inserted underneath. The flap was then sutured with nonabsorbable 4.0 sutures, anchoring the silicone in place.

Animals were randomly assigned to 3 timepoint groups (5, 7, and 14 days), and wounds were randomly divided into 5 treatment groups ($n \geq 7$), namely CMC, CMC-SF, CMC-GH, CMC-SF-GH (washed), and non-treated wounds as a control group. Each dressing was individually applied and secured with a transparent adhesive film (3M Tegaderm) to protect the wound site and ensure the dressing remained in place, preventing interference or removal by the animals. The adhesive film was replaced every other day to maintain hygiene and dressing integrity. Post-surgery, animals were housed individually. Buprenorphine HCl (0.05 mg kg^{-1}) was administered subcutaneously on the day of surgery and after 24 and 48 h from the surgery. Wound area was measured using digital photographs taken at specific timepoints. The images were analyzed with ImageJ software (NIH; Bethesda, MD, USA). The wound closure rate was calculated using Equation (2):

$$\text{Wound closure} \quad (\%) = 100 \times \frac{\text{Wound area at } t_0 - \text{Wound area } t_t}{\text{Wound area at } t_0} \quad (2)$$

Animals were euthanized at specific timepoints (5, 7, or 14 days) by CO_2 inhalation followed by cervical dislocation. Tissue samples (8 mm diameter, $n = 3$) were collected, washed with sterile saline, and fixed in 4% paraformaldehyde for histopathological (H&E) and immunohistochemical (CD31, PCNA) analysis. Samples were cryoprotected with 30% w/v saccharose, embedded in OCT compound (Tissue-Tek, Sakura Finetek), and frozen with liquid-nitrogen-cooled isopentane. Sections (20 µm) were obtained with a cryostat, mounted on Superfrost Plus (Menzel-Glasser, Madison, WI, USA) slides, and analyzed. Details are described in Section S2.3 (Supporting Information). The quantitative analysis of the number of proliferating cells (PCNA) and newly formed vessels (CD31) was conducted using ImageJ software (NIH, Bethesda, MD) based on microscopy images. For protein extraction, tissue explants were frozen at –80 °C (Section S2.4, Supporting Information).

Proteomic Analysis by LC-MSM: Proteomic analysis was performed using a micro-LC-MS/MS (Eksigent nanoLC 400 or nLC425, SCIEX) coupled to a Triple TOF 6600 mass spectrometer. Proteins (100 µg per sample) were separated by SDS-PAGE, stained with Sypro-Ruby, and submitted to an in-gel tryptic digestion,[87] as detailed in Section S2.4 (Supporting Information).

Qualitative Analysis by DDA (Dependent Data Analysis): After digestion, peptides were resuspended in 0.1% formic acid (mobile phase A) by sonication, and 4 µL of each sample were injected into a YMC TRIART C18 reversed-phase guard column connected online to an analytical C18 column (150 × 0.30 mm, 3 µm, 120 Å). Peptide separation was achieved at a flow rate of 5 µL min^{-1} using a 90-min linear gradient from 2% to 90% mobile phase B (acetonitrile with 0.1% formic acid).

The mass spectrometer operated in positive ion mode using data-dependent acquisition (DDA). Survey MS scans were acquired over an m/z range of 400–1250 (250 ms), followed by MS/MS scans (m/z 100–1500, 25 ms) of the top 65 precursor ions per cycle (2.8 s total). Precursors were selected based on charge (+ 2 to + 5), m/z (350–1400), and intensity (>200 cps), with a dynamic exclusion window of 15 s. Singly charged ions were excluded. Instrument calibration was automatically performed every 4 h using the SCIEX pepCalMix. Data analysis was carried out using ProteinPilot 5.0.2 (SCIEX) with the Paragon algorithm for protein identification and ProGroup for protein grouping, searching against a rat-specific UniProt database using carbamidomethylation of cysteine as a fixed modification and applying a 1% false discovery rate (FDR) for both peptide and protein identification. Semi-quantitative analysis was conducted with Scaffold DDA (v6.4.1) based on spectral counting[88] (more details in Section S2.4, Supporting Information).

Quantitative Analysis by SWATH-MS (Sequential Window Acquisition of all Theoretical Mass Spectra-DIA) Method: The MS/MS spectral libraries were created using a data-dependent acquisition (DDA) approach by micro-LC-MS/MS as previously described.[89–94] Equal peptide amounts from each treatment group were pooled and analyzed under the same DDA conditions. Peptides per pool (4 µg) were run on the nLC425 system using a 40-min linear gradient (5% to 95% mobile phase B), followed by MS analysis on the Triple TOF 6600.

Data were processed using ProteinPilot (v5.0.1/5.0.2) as described previously to obtain the MSMS library. For quantitative analysis, Sequential Window Acquisition of all Theoretical Mass Spectra (SWATH-MS) acquisition was performed on individual samples using 100 variable-width DIA windows spanning m/z 400–1250. Fragment ion chromatograms were extracted with PeakView 2.2 (SWATH MicroApp) and analyzed in MarkerView. Up to 10 peptides and 7 fragments per protein were quantified. Statistical comparisons were performed using normalized peak areas and Student's *t*-test (detailed in Section S2.4, Supporting Information).

Proteomic Data Analysis: Venn diagrams were generated from Scaffold DDA data using SRplot software (https://www.bioinformatics.com.

cn/en). Furthermore, differentially expressed proteins were represented by comparing 2 conditions per graph using Volcano Plots, created in Prism (GraphPad software, La Jolla, CA, USA). Heatmaps were elaborated to compare the effect of SF and GH presence. Proteins with $p < 0.05$ were represented using the fold change values to compare the conditions and plotted using Heatmapper software (http://www.heatmapper.ca/expression/). Functional analysis and protein interaction were performed using string (https://string-db.org/) using a minimum interaction score of high confidence (0.700).

Statistical Analysis: Statistical analysis was carried out using Prism (GraphPad Software; La Jolla, CA, USA). All data were expressed as mean ± standard deviation. One-way analysis of variance (ANOVA) and Tukey's multiple comparison post-test were used. Differences were considered significant for $p < 0.05$.

Supporting Information

Supporting Information is available from the Wiley Online Library or from the author.

Acknowledgements

The authors would like to thank Cristian Rojas for the assistance during the in vivo experiment and Carmen Pena for the help with protein extraction and digestion. M.P-V. acknowledges Xunta de Galicia for a predoctoral contract [ED481A-2023-164]. D.C-V. acknowledges IDIS collaboration for the development of the in vivo experiments. The work was supported by Spain Ministerio de Ciencia, Innovación y Universidades MICIU/AEI/10.13039/501100011033 [PID2021-127493OA-C22, CNS2023-145568, and PID2023-150422OB-I00], ERDF A way of making Europe, cofunded by the European Union, Xunta de Galicia [ED431C 2024/09]. This work has been partially supported by the European Commission ERDF/FEDER Operational Programme of Murcia (2021-2027) [Project No. 50463] "Development of sustainable models of agricultural, livestock and aquaculture production" (Subproject: Innovation in the field of sericulture: New materials, biomaterials and extracts of biomedical interest).

Conflict of Interest

The authors declare no conflict of interest.

Data Availability Statement

The data that support the findings of this study are available from the corresponding author upon reasonable request.

Keywords

3D printing, growth hormone, ischemic wounds healing, personalized dressings, proteomics

Received: June 12, 2025
Revised: October 3, 2025
Published online:

[1] J. Qin, F. Chen, P. Wu, G. Sun, *Bioeng. Biotechnol.* **2022**, *10*, 841583.
[2] E. R Ghomi, M. Niazi, S. Ramakrishna, *Adv. Tech.* **2023**, *34*, 520.
[3] R. Frykberg, J. Banks, *Adv. Wound Care* **2015**, *4*, 560.
[4] A. G. Tabriz, D. Douroumis, *J. Drug Deliv. Sci. Technol.* **2022**, *74*, 103564.
[5] E. M. Tottoli, R. Dorati, I. Genta, E. Chiesa, S. Pisani, B. Conti, *Pharmaceutics* **2020**, *12*, 735.
[6] S. M. Lee, I. K. Park, Y. S. Kim, H. J. Kim, H. Moon, S. Mueller, Y.-I. L. Jeong, *Biomater. Res.* **2016**, *20*, 15.
[7] D. Diekjürgen, D. W. Grainger, *Biomaterials* **2017**, *141*, 96.
[8] M. Milojevic, G. Harih, B. Vihar, J. Vajda, L. Gradisnik, T. Zidaric, K. Stana Kleinschek, U. Maver, T. Maver, *Pharmaceutics* **2021**, *13*, 564.
[9] A. Francesko, P. Petkova, T. Tzanov, *Med. Chem.* **2018**, *25*, 5782.
[10] M. Gholipourmalekabadi, S. Sapru, A. Samadikuchaksaraei, R. L. Reis, D. L. Kaplan, S. C. Kundu, *Adv. Drug Delivery Rev.* **2020**, *153*, 28.
[11] H. Shao, Z. Sun, *Polym. Bull.* **2023**, *81*, 3759.
[12] G. Lee, Y.-G. Ko, K. H. Bae, M. Kurisawa, O. K. Kwon, O. H. Kwon, *Biomater. Res.* **2022**, *26*, 62.
[13] L. Wei, S. Wu, M. Kuss, X. Jiang, R. Sun, P. Reid, X. Qin, B. Duan, *Bioact. Mater.* **2019**, *4*, 256.
[14] Z. Akdag, S. Ulag, D. M. Kalaskar, L. Duta, O. Gunduz, *Biomimetics* **2023**, *8*, 612.
[15] C. You, C. Wang, Z. Ma, Q. Yu, S. Liu, *Int. J. Biol. Macromol.* **2025**, *298*, 140082.
[16] A. P. Madappura, S. Madduri, *Comput. Struct. Biotechnol. J.* **2023**, *21*, 4868.
[17] M. Pita-Vilar, A. Concheiro, C. Alvarez-Lorenzo, L. Diaz-Gomez, *Carbohydr. Polym.* **2023**, *321*, 121298.
[18] X. Wang, J. Qi, W. Zhang, Y. Pu, R. Yang, P. Wang, S. Liu, X. Tan, B. Chi, *Int. J. Biol. Macromol.* **2021**, *187*, 91.
[19] L. Diaz-Gomez, I. Gonzalez-Prada, R. Millan, A. D. Silva-Candal, A. Bugallo-Casal, F. Campos, A. Concheiro, C. Alvarez-Lorenzo, *Carbohydr. Polym.* **2022**, *278*, 118924.
[20] D. Caicedo, P. Devesa, C. V. Alvarez, J. Devesa, *Cells* **2020**, *9*, 807.
[21] Z. Garoufalia, A. Papadopetraki, E. Karatza, D. Vardakostas, A. Philippou, G. Kouraklis, D. Mantas, *Biomed. Rep.* **2021**, *15*, 66.
[22] S. W. Lee, S. H. Kim, J. Y. Kim, Y. Lee, *J. Plast., Reconstr. Aesthet. Surg.* **2010**, *63*, 364.
[23] R. Ajo, L. Cacicedo, C. Navarro, F. Sánchez-Franco, *Endocrinology* **2003**, *144*, 1086.
[24] L. Cristobal, N. de Los Reyes, M. A. Ortega, M. Alvarez-Mon, N. Garcia-Honduvilla, J. Bujan, A. A. Maldonado, *Int. J. Mol. Sci.* **2019**, *20*, 4157.
[25] D. Valdés, P. Devesa, V. Arce, J. Requena, J. Devesa, *Ther. Adv. Cardiovasc. Dis.* **2018**, *12*, 53.
[26] S. Spiliopoulos, G. Festas, I. Paraskevopoulos, M. Mariappan, E. Brountzos, *World J. Diabetes* **2021**, *12*, 2011.
[27] J. Broadbent, T. Walsh, Z. Upton, *Proteomics Clin. Appl.* **2010**, *4*, 204.
[28] L. Stolzenburg-Veeser, O. Golubnitschaja, *J. Proteomics* **2018**, *188*, 71.
[29] M. Chang, T. T. Nguyen, *Chem. Res.* **2021**, *54*, 1080.
[30] Y. Wang, Y. Pi, L. Hu, Z. Peng, H. Hu, J. Zhao, Y. Zhou, D. Wang, *Biol. Med.* **2023**, *159*, 106858.
[31] Ł. Mazurek, M. Szudzik, M. Rybka, M. Konop, *Biomolecules* **2022**, *12*, 1852.
[32] G. F. de Lima, A. G. de Souza, D. S. Rosa, *Macromol. Symp.* **2020**, *394*, 2000126.
[33] C. B. Highley, C. B. Rodell, J. A. Burdick, *Adv. Mater.* **2015**, *27*, 5075.
[34] E. R. Johnston, Y. Miyagi, J. A. Chuah, K. Numata, M. A. Serban, *ACS Biomater. Sci. Eng.* **2018**, *4*, 2815.
[35] J. Kundu, R. Mohapatra, S. C. Kundu, *J. Biomater. Sci., Polym. Ed.* **2011**, *22*, 519.
[36] Y. Wei, D. Sun, H. Yi, J. Wang, *Text. Res. J.* **2014**, *84*, 959.
[37] S. Chankow, S. Luemunkong, S. Kanokpanont, presented at *2016 9th Biomedical Engineering Int. Conf. (BMEiCON)*, Laung Prabang, Laos, December **2016**.

[38] V. P. Ribeiro, J. Silva-Correia, C. Goncalves, S. Pina, H. Radhouani, T. Montonen, J. Hyttinen, A. Roy, A. L. Oliveira, R. L. Reis, J. M. Oliveira, *PLoS One* **2018**, *13*, 0194441.
[39] S. Sakai, T. Morita, *Biomater. Sci. Eng.* **2022**, *8*, 2589.
[40] W. Sun, D. A. Gregory, M. A. Tomeh, X. Zhao, *Int. J. Mol. Sci.* **2021**, *22*, 1499.
[41] R. Rakhshaei, H. Namazi, *Mater. Sci. Eng. C* **2017**, *73*, 456.
[42] P. Basu, U. Narendrakumar, R. Arunachalam, S. Devi, I. Manjubala, *ACS Omega* **2018**, *3*, 12622.
[43] S. Wang, Q. Han, D. Zhang, J. Liu, Z. Shen, X. Wei, X. Li, *Express* **2022**, *12*, 1572.
[44] M. He, F. Ou, Y. Wu, X. Sun, X. Chen, H. Li, D. Sun, L. Zhang, *Mater. Des.* **2020**, *194*, 108913.
[45] P. Farshi, R. Salarian, M. Rabiee, S. Alizadeh, M. Gholipourmalekabadi, S. Ahmadi, N. Rabiee, *Polym. Eng. Sci.* **2022**, *62*, 2741.
[46] Z. Lan, R. Kar, M. Chwatko, E. Shoga, E. Cosgriff-Hernandez, *J. Biomed. Mater. Res., Part A* **2023**, *111*, 465.
[47] S. A. Razack, Y. Lee, H. Shin, S. Duraiarasan, B.-S. Chun, H. W. Kang, *Int. J. Biol. Macromol.* **2023**, *226*, 220.
[48] Y. Shan, C. Li, Y. Wu, Q. Li, J. Liao, *RSC Adv.* **2019**, *9*, 22966.
[49] M. Tavakolian, J. G. Munguia-Lopez, A. Valiei, M. S. Islam, J. M. Kinsella, N. Tufenkji, T. G. M. van de Ven, *ACS Appl. Mater. Interfaces* **2020**, *12*, 39991.
[50] K. Nuutila, E. Eriksson, *Adv. Wound Care* **2020**, *10*, 685.
[51] T. Karimi, F. Mottaghitalab, H. Keshvari, M. Farokhi, *J. Drug Deliv. Sci. Tech.* **2023**, *80*, 104134.
[52] S. Khosravimelal, M. Chizari, B. Farhadihosseinabadi, M. Moosazadeh Moghaddam, M. Gholipourmalekabadi, *J. Mater. Sci. Mater. Med.* **2021**, *32*, 114.
[53] AENOR, Test methods for primary wound dressings: Part 2: Moisture vapour transmission rate of permeable film dressings UNE-EN 13726-2:2002, **2003**.
[54] T. C. Trevisol, A. R. M. Fritz, S. M. A. G. U. de Souza, A. C. K. Bierhalz, J. A. B. Valle, *J. Appl. Polym. Sci.* **2019**, *136*, 46941.
[55] D. Chouhan, B. Chakraborty, S. K. Nandi, B. B. Mandal, *Acta Biomater.* **2017**, *48*, 157.
[56] A. Habib, V. Sathish, S. Mallik, B. Khoda, *Materials* **2018**, *11*, 454.
[57] V. R. Shah, P. K. Gupta, *Pharm. Res.* **2018**, *35*, 98.
[58] J. Buijs, D. W. Britt, V. Hlady, *Langmuir* **1998**, *14*, 335.
[59] R. Ajo, L. Cacicedo, C. Navarro, F. Sánchez-Franco, *Endocrinology* **2003**, *144*, 1086.
[60] T. Del Pino-Sedeno, M. M. Trujillo-Martin, I. Andia, J. Aragon-Sanchez, E. Herrera-Ramos, F. J. Iruzubieta Barragan, P. Serrano-Aguilar, *Wound Repair Regen.* **2019**, *27*, 170.
[61] R. Guillamat-Prats, *Cells* **2021**, *10*, 1729.
[62] E. Ranzato, M. Patrone, L. Mazzucco, B. Burlando, *Br. J. Dermatol.* **2008**, *159*, 537.
[63] K. Matsuura, T. Kuratani, T. Gondo, A. Kamimura, M. Inui, *Eur. J. Pharmacol.* **2007**, *563*, 83.
[64] Y. Guan, F. Sun, X. Zhang, Z. Peng, B. jiang, M. Liang, Y. Wang, *J. Mater. Sci.: Mater. Med.* **2020**, *31*, 48.
[65] M. K. Rausch, S. H. Parekh, B. Dortdivanlioglu, A. M. Rosales, *Prog. Biomed. Eng.* **2021**, *3*, 042006.
[66] E. Grambow, H. Sorg, C. G. G. Sorg, D. Strüder, *Med. Sci.* **2021**, *9*, 55.
[67] M. Shahriari-Khalaji, M. Sattar, R. Cao, M. Zhu, *Bioact. Mater.* **2023**, *29*, 177.
[68] G. Merckx, H. Tay, M. L. Monaco, M. van Zandvoort, W. De Spiegelaere, I. Lambrichts, A. Bronckaers, *Tissue Eng., Part B* **2020**, *26*, 519.
[69] K. M. Marshall, J. M. Kanczler, R. O. Oreffo, *J. Tissue Eng.* **2020**, *11*, 2041731420942734.
[70] A. N. Trujillo, S. L. Kesl, J. Sherwood, M. Wu, L. J. Gould, *J. Vis. Exp.* **2015**, *98*, 52637.
[71] D. Singh, V. Rai, D. K. Agrawal, *Cardiol. Cardiovasc. Med.* **2023**, *7*, 5.
[72] Y. Xiang, L. Li, S. Xia, J. Lv, X. Li, *Bioengineered* **2021**, *12*, 9463.
[73] N. Potere, M. G. Del Buono, G. Niccoli, F. Crea, S. Toldo, A. Abbate, *Int. J. Mol. Sci.* **2019**, *20*, 544.
[74] C. Peng, H. Xu, Q. Zhuang, J. Liu, Y. Ding, Q. Tang, Z. Wang, K. Yao, *Wound Repair Regener.* **2024**, *32*, 638.
[75] K. Huang, B. Mi, Y. Xiong, Z. Fu, W. Zhou, W. Liu, G. Liu, G. Dai, *Burns Trauma* **2025**, *13*, tkae052.
[76] M. M. Martino, P. S. Briquez, A. Ranga, M. P. Lutolf, J. A. Hubbell, *Proc. Natl. Acad. Sci. USA* **2013**, *110*, 4563.
[77] K.-Y. Cheng, Z.-H. Lin, Y.-P. Cheng, H.-Y. Chiu, N.-L. Yeh, T.-K. Wu, J.-S. Wu, *Sci. Rep.* **2018**, *8*, 12214.
[78] A. Bouter, C. Gounou, R. Bérat, S. Tan, B. Gallois, T. Granier, B. L. d'Estaintot, E. Pöschl, B. Brachvogel, A. R. Brisson, *Nat. Commun.* **2011**, *2*, 270.
[79] M. B. Zaidi, F. Khan, F. Jameel, I. Khan, S. G. Musharraf, A. Salim, *Cell Biochem. Funct.* **2024**, *42*, 3946.
[80] S. Wu, C. Ma, S. Shan, L. Zhou, W. Li, *Sci. Rep.* **2017**, *7*, 46531.
[81] R. Surolia, F. J. Li, Z. Wang, H. Li, K. Dsouza, V. Thomas, S. Mirov, D. Pérez-Sala, M. Athar, V. J. Thannickal, V. B. Antony, *JCI Insight* **2019**, *4*, 123253.
[82] M. Najberg, M. Haji Mansor, T. Taillé, C. Bouré, R. Molina-Peña, F. Boury, J. L. Cenis, E. Garcion, C. Alvarez-Lorenzo, *Carbohydr. Polym.* **2020**, *237*, 116107.
[83] J. Conceicao, X. Farto-Vaamonde, A. Goyanes, O. Adeoye, A. Concheiro, H. Cabral-Marques, J. M. Sousa Lobo, C. Alvarez-Lorenzo, *Carbohydr. Polym.* **2019**, *221*, 55.
[84] M. V. Konovalova, P. A. Markov, E. A. Durnev, D. V. Kurek, S. V. Popov, V. P. Varlamov, *J. Biomed. Mater. Res., Part A* **2017**, *105*, 547.
[85] M. Li, Z. Zhang, Y. Liang, J. He, B. Guo, *ACS Appl. Mater. Interfaces* **2020**, *12*, 35856.
[86] X. Farto-Vaamonde, L. Diaz-Gomez, A. Parga, A. Otero, A. Concheiro, C. Alvarez-Lorenzo, *J. Control. Release.* **2022**, *352*, 776.
[87] A. Shevchenko, M. Wilm, O. Vorm, M. Mann, *Anal. Chem.* **1996**, *68*, 850.
[88] I. V. Shilov, S. L. Seymour, A. A. Patel, A. Loboda, W. H. Tang, S. P. Keating, C. L. Hunter, L. M. Nuwaysir, D. A. Schaeffer, *Mol. Cell. Proteomics* **2007**, *6*, 1638.
[89] J. V. Álvarez, S. B. Bravo, M. P. Chantada-Vázquez, C. Pena, C. Colón, S. Tomatsu, F. J. Otero-Espinar, M. L. Couce, *Int. J. Mol. Sci.* **2024**, *25*, 3232.
[90] T. Blanco-Pintos, A. Regueira-Iglesias, M. Relvas, M. Alonso-Sampedro, S. B. Bravo, C. Balsa-Castro, I. Tomás, *J. Clin. Periodontol.* **2025**, *52*, 199.
[91] A. Bugallo-Casal, E. Muiño, S. B. Bravo, P. Hervella, S. Arias-Rivas, M. Rodríguez-Yáñez, E. Vara-León, R. Quintas-Rey, L. Pérez-Gayol, O. Maisterra-Santos, J. Pizarro-Gonzálvez, M. R. Martorell-Riera, C. Vives-Bauzá, I. Fernández-Cadenas, J. Castillo, F. Campos, *NeuroMol. Med.* **2025**, *27*, 18.
[92] P. Mondelo-Macía, J. García-González, L. León-Mateos, A. Abalo, S. Bravo, M. d P Chantada Vazquez, L. Muinelo-Romay, R. López-López, R. Díaz-Peña, A. B. Dávila-Ibáñez, *Mol. Cell. Proteomics.* **2024**, *23*, 100834.
[93] R. Picáns-Leis, M. E. Vázquez-Mosquera, M. Pereira-Hernández, M. Vizoso-González, L. López -Valverde, S. Barbosa-Gouveia, O. López-Suárez, C. López-Sanguos, S. B. Bravo, M. A. García-González, M. L. Couce, *Clin. Nutr.* **2025**, *44*, 178.
[94] J. S. Rodrigues, M. Chenlo, S. B. Bravo, S. Perez-Romero, M. Suarez-Fariña, T. Sobrino, R. Sanz-Pamplona, R. González-Prieto, M. N. Blanco Freire, R. Nogueiras, M. López, L. Fugazzola, J. M. Cameselle-Teijeiro, C. V. Alvarez, *Nat. Commun.* **2024**, *15*, 3736.